**SIRM 2015 – 11th International Conference on Vibrations in Rotating Machines,
Magdeburg, Deutschland, 23. – 25. February 2015**

Chaotic and stable orbits of a rotor in a non-conventional back-up bearing. A numerical and experimental approach

Cesar A.L.L. Fonseca[1], **Romulo R. Aguiar**[2], **Hans I. Weber**[2]

[1] Department of Mechanical Engineering, Technical University of Denmark, Nils Koppels Alle Bygning 404, DK-2800, Kgs. Lyngby, Denmark, cefonse@dtu.dk
[2] Department of Mechanical Engineering, PUC-Rio, Rua Marquês de São Vicente, 225, Rio de Janeiro, Brazil, 22451-900, hans@puc-rio.br

Abstract

The present work is a numerical study with experimental validation of the non-linear behaviour of a rotor interacting with a non-conventional stator bearing. When the rotor's movement in the (x, y) plane reaches an undesirable amplitude, such movement is restrained by the non-conventional stator, composed by pins. These pins receive all the impacts, working as a containment bearing. While conducting numerical simulations, the results show the different characteristics of the rotor orbit, depending on the applied torque. The steady state trajectories formed singular geometries, different from each other. A considerable set of data was collected, showing this interesting rotor/stator interaction due to impacts with the pins. The results include various non-linear features, such as bifurcations and chaos. Furthermore an experimental test rig is mounted and the position of the rotor inside the modified safety bearing is measured and the result is compared to the simulation presented.

1 Introduction

Rotor/stator contact is one of the most serious malfunctions occurring in rotating machinery. Specifically, rotor rub against a seal may lead to a catastrophic failure of the machine in a very short time. The rotor/stator rub may manifest itself in the form of a full annular rub, when the contact between the rotor and stator is maintained continuously. The rub occurs due to high friction-related wear and damage may occur quite rapidly. The topic of full annular rub and dry whip recently gained more attention, following an increasing number of applications of machines with active magnetic bearings, usually equipped by retainer bearings (Muszynska [1]).

Retainer bearings (also called *back-up*, *auxiliary* or *safety* bearings) have become standard 'back-up' elements in rotor machinery applications. They provide support for the machine rotor during start-ups and shut-downs. Recently, retainer bearings have been using not only for these functions, which are auxiliary to the machine main operation, but also in "load-sharing" applications. In these uses, while not interfering with the rotor during normal machine operation, retainer bearings provide added, often just temporary, support to the rotor in critical situations. Sudden imbalance or bearing failure give rise to transient short- or long-term overloads, which would lead to rotor increased lateral static or dynamic displacements of the rotor. The use of retainer bearings as an additional load-sharing support of the rotor during all abnormal conditions must ensure safe, effective, and consistent operation of the machine.

The dynamic phenomena occurring when the rotor is forced to get into contact with the retainer bearings are very similar to the rotor full annular rubs in mechanical seals and/or other stationary contacting parts with circumferential surfaces. The regime of self-excited dry whip of a rotor dropped onto retainer bearings is certainly very unwelcome, and can be devastating [2]. Impacts and rubbing are also a major concern for magnetic bearings machines, which a sudden failure or due to a non-robust control is considered a critical issue as the rotor looses its levitation support. Magnetic bearing designs are described by Schweizter [3] and Ulbrich [4] and since then it has become a device with great importance and industrial interest. Therefore, the eventual drop of a rotor on the bearing and ways to avoid contact on the structure are densely researched.

While the rotor/retainer bearing dynamic behaviour was addressed in several publications (e.g., [5]-[8]), the aspect of designed load-sharing feature of these bearings during normal operations only recently became the subject of research. Retainer bearings with pins inside the structure were developed for this purpose.The idea of using pins to reduce the rotor amplitude was primarily investigated by graduate students in the Dynamics and Vibration

Laboratory at PUC-Rio. The ongoing cooperation with DTU (Denmark Technical University) lead to the results presented by Lahriri ([14]-[15]), Fonseca [9, 11]. They conducted numerical and experimental analyses of a rotor system with the presence of the pins in safety bearings. One main purpose of that retainer bearing design is to prevent the whirling effect on the rotor interacting with the stator. Such phenomenon, especially if a backward whirl arises, is hazardous, leading to shaft fatigue and bearing or rotor failure. The idea behind the presence of the pins is that they act as elements to support impacts. In [9], a controlled, but rather simplified concept of a bearing design using pins, showed that this safety bearing design could help the rotor to surpass its critical speed. The controller acts by advancing the pins into the bearing clearance during critical situations, such as the rotor reaching resonance or rotor amplitudes high enough that impacts on the bearing wall may occur. When the rotor returns to a low vibration condition or no other indication of rotor instability exists, the pins are retracted, and the rotor resumes its normal operation. The simulations, combined with experimental validation, showed that it is possible to overcome the rotor critical speed with the help of this new safety bearing. Nevertheless, the torque must be greater than the minimum torque [17] necessary to overcome this operation point.

The impact behaviour of the disk was previously analysed in the work of Isaksson [13], which identifies stable regions by various parameters.

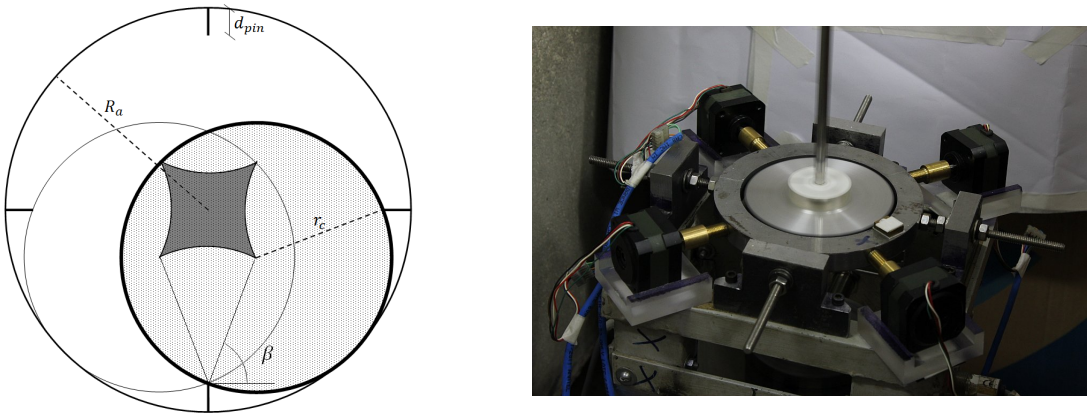

(a) (b)

Figure 1: (a) Sketch of the safety bearing design using impact pins to avoid rubbing. The grey area is the rotor center free area, or workspace. (b) Prototype of the safety bearing on the rotor machinery test rig.

In this work a numerical study takes place to investigate the shape of the orbits and the impact force magnitudes during the rotor start up, under different motor torque values (even lower than the minimum torque). Due to the presence of the strong non-linearity caused by the impacts, the mechanical system presents different and unique orbit shapes, even under the slightest variations of the applied torque. Bifurcations and chaotic behaviours are also observed by mapping the impact forces magnitudes and the disk center position in time. Due to the strong non-linearity caused by the impacts at the steady state, a slight increase or decrease in the motor torque can result in a different form of the trajectory of the disk center. Also, the forces on the pins at each impact are calculated and the next steps include a comparison of these numerical studies with experimental results (Prototype of safety bearing shown in Figure 1(b)).

2 Theoretical approach

In order to model the experimental test rig shown in Figure 1(b), the hypothesis of massless shaft is used, along with the fact that gyroscopic effects are neglected. Therefore, the modelling of the rotor when not impacting the pins is the classical DeLaval modelling, a well-known rotor dynamics set up equations found in the rotordynamics literature [12]. With the parameters defined in Figure 2(a) the equations of motion are

$$\begin{cases} m\ddot{x}(t) + c_1\dot{x}(t) + k_1 x(t) = m\varepsilon\ddot{\theta}(t)\sin\theta(t) + m\varepsilon\dot{\theta}^2\cos\theta(t), \\ m\ddot{y}(t) + c_1\dot{y}(t) + k_1 y(t) = -m\varepsilon\ddot{\theta}(t)\cos\theta(t) + m\varepsilon\dot{\theta}^2\sin\theta(t), \\ mR_g^2\ddot{\theta}(t) = T(\dot{\theta}) - k_1\varepsilon x(t)\sin\theta(t) + k_1\varepsilon y(t)\cos\theta(t), \end{cases} \tag{1}$$

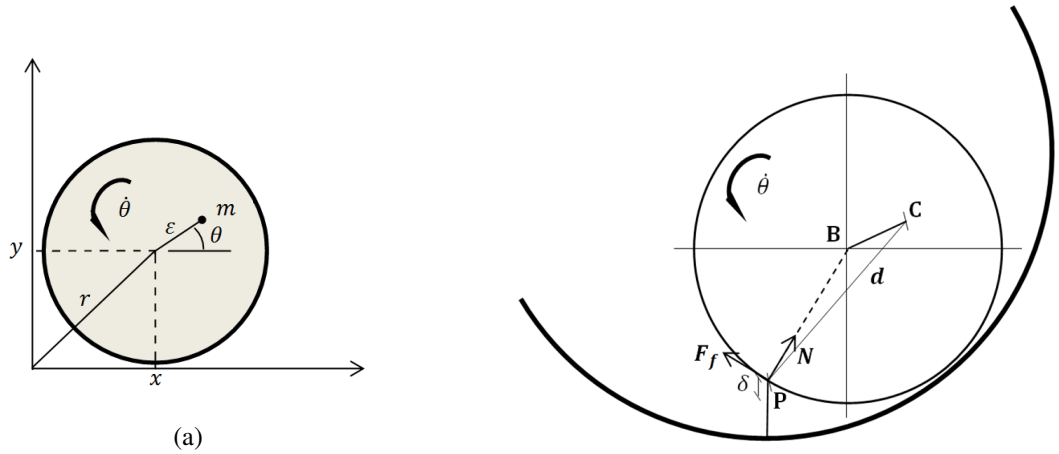

(a) (b)

Figure 2: (a) Rotor parametrization. (b) The rotor-pin contact state.

where the rotor parameters are its mass *m*, gyration radius R_g and rotor eccentricity ε. The shaft presents stiffness k_1 and damping c_1.

The presence of the pins leads to a discontinuity in the dynamical equations due to the impact force. The pins are considered small one-dimensional bars, which deform only along its length, *i.e.*, the pins do not suffer the effects of buckling or lateral deformation and can resist fatigue and strong impacts. For modelling purposes, the pins are considered as spring elements. The contact state is modelled as a spring element coupled to a dry friction force (Coulomb friction), acting on the edge of the disk, see Figure 2(b).

Mathematically, the contact state happens when the distance from the disk center to the top of the i-th pin is smaller than the disk radius, Eq. (2):

$$\eta_i = \mathbf{P}_i - \mathbf{B} = \begin{cases} \mathbf{r}_{PB} - R_d \leq 0 \rightarrow \text{impact}; & \eta_i = 1 \\ \mathbf{r}_{PB} - R_d > 0 \rightarrow \text{no impact}; & \eta_i = 0, \end{cases} \tag{2}$$

where η_i denotes an impact on top of the *i*th pin to disk center **B**. This is an arbitrary convention which determines the sign of the impact formulation.

Although it is assumed that the pins deflect only in its axial direction, the impact force on the disk is directed from the contact point to the center of the disk, due to the geometry of the impact. Therefore, when the disk starts impacting on one of the pins, the angle of impact incidence β must be calculated, in the fixed reference frame, see Figure 1(a). Thus, the impact force vector $\mathbf{N}$ has the components

$$\mathbf{N} = \begin{pmatrix} N_x \\ N_y \\ 0 \end{pmatrix} = \begin{pmatrix} |\mathbf{N}| \cos\beta \\ |\mathbf{N}| \sin\beta \\ 0 \end{pmatrix}; |\mathbf{N}| = K_p |\boldsymbol{\delta}|, \tag{3}$$

where δ is the pin deformation and K_p is the pin stiffness.

Along with the impact, the friction effect is also considered, modelled as a Coulomb friction. The friction force is orthogonal with respect to the normal force. Since the center of mass is displaced from the center of the disk, there is a torque applied from the normal force besides the torque of the friction force. The vectorial parameter $\mathbf{d}$ in Figure 2(b) is the distance between the disk center of mass and the contact point. Therefore, the influence of the pins is considered as a punctual element inside the retainer bearing structure. A small quadratic damping term was added to the torque function to limit the angular velocity, when it reaches a far greater speed above the critical one. The dynamical equations with impacts are

$$\begin{cases} m\ddot{x} + c_1\dot{x} + k_1 x = m\varepsilon\ddot{\theta}\sin\theta + m\varepsilon\dot{\theta}^2\cos\theta + \eta_i\left(N_x + N_y\mu\,\mathrm{sign}(\mathrm{V_{edge,x}})\right), \\ m\ddot{y} + c_1\dot{y} + k_1 y = -m\varepsilon\ddot{\theta}\cos\theta + m\varepsilon\dot{\theta}^2\sin\theta - \eta_i\left(N_y + N_x\mu\,\mathrm{sign}(\mathrm{V_{edge,y}})\right), \\ mR_g^2\ddot{\theta} = T(\dot{\theta}) - k_1\varepsilon x\sin\theta + k_1\varepsilon y\cos\theta + \eta_i\left(|\mathbf{d}\times\mathbf{N}| - \mu|\mathbf{d}\times\mathbf{F}|\frac{\mathrm{V_{edge}}}{|\mathrm{V_{edge}}|}\right), \end{cases} \tag{4}$$

where $\mathrm{V_{edge}}$ is the velocity vector on the impacting edge of disk.

It is important to point out that in our modelling that the rotor's angular velocity is not constant. It accelerates with a constant applied motor torque T and may decelerate due to impact interactions with the pins. If the torque is not high enough, the rotor may not surpass the critical speed.

The reactive impact forces on the pins are modelled as linear elastic, whose magnitude is proportional to the penetration δ of the rotor on the pin. All model parameters of the test rig were identified in previous works [9]-[10].

In the following step, equation (4) is written in dimensionless terms, so all spatial coordinates and parameters are divided by the unbalanced eccentricity ε. The time domain was also parametrized using the natural frequency term ω. Equations (1) and (4) can be considered as a set of ordinary differential equations with a discontinuous right-hand side. They were normalized using the following rules: $X = x/\varepsilon$, $Y = y/\varepsilon$ and $\tau = \omega t$ with $\omega = \sqrt{k_1/m}$. Equation (1) is rewritten as

$$\begin{cases} X'' + X = \theta''\sin\theta + \theta'^2\cos\theta, \\ Y'' + Y = -\theta''\cos\theta + \theta'^2\sin\theta, \\ \theta'' = \frac{T}{1/2mR_g^2\omega^2} + \left(\frac{\varepsilon}{R_g}\right)^2(Y\cos\theta - X\sin\theta) \end{cases} \tag{5}$$

and Equation (4) as

$$\begin{cases} X'' + X = \theta''\sin\theta + \theta'^2\cos\theta + \eta_i\left[\left(\frac{\omega_p}{\omega}\right)^2\frac{\delta_x}{\varepsilon} + \left(\frac{\omega_p}{\omega}\right)^2\frac{\delta_y}{\varepsilon}\mu\ \mathrm{sign}(V^\star_{edge,x})\right], \\ Y'' + Y = -\theta''\cos\theta + \theta'^2\sin\theta - \eta_i\left[\left(\frac{\omega_p}{\omega}\right)^2\frac{\delta_y}{\varepsilon} + \left(\frac{\omega_p}{\omega}\right)^2\frac{\delta_x}{\varepsilon}\mu\ \mathrm{sign}(V^\star_{edge,y})\right], \\ \theta'' = \bar{T} + \left(\frac{\varepsilon}{R_g}\right)^2(Y\cos\theta - X\sin\theta) + \eta_i\left[\frac{2}{R_g^2}\left(\frac{\omega_p}{\omega}\right)^2|\mathbf{d}\times\boldsymbol{\delta}|\left(1 - \mu\frac{V^\star_{edge}}{|V^\star_{edge}|}\right)\right], \end{cases} \tag{6}$$

where the time derivative is replaced by $\frac{d}{dt}X = \omega X'$ and $\omega_p = \sqrt{K_p/m}$ and $\bar{T} = \frac{T}{1/2mR_g^2\omega^2}$ are introduced. Now that we have the contact equations dimensionless, simulations with different dimensionless rotor parameters may be compared. All the simulation results will be shown using dimensionless parameters.

3 Simulations' results

In the following, the sets of equations, (5) and (6), were solved using a variable step Runge-Kutta method (implemented in the *ode45* solver in *Matlab*). Along with the *ode45* solver, a separate programming routine was developed in order to identify on which pin the disk is impacting during the contact state, and then it calculates the impact incident angle β. Additionally, this routine provides the impact force and torque during each contact state. Proper analysis of the error tolerances was performed in order to consistently integrate such mathematical sets of equations. The parameters used in the simulations were taken from the experimental test rig [9].

As mentioned earlier, the idea is to evaluate the system behaviour during the rotor start up, having as inputs the dimensionless torque of the motor (divided by the minimum torque T_a, shown in Equation (7), see [12]) and the size of the free motion of the rotor (grey area in Figure 1(a)), defined by one parameter: the impact gap, *i.e.*, the geometric relationship between rotor and stator radius and the pins' lengths. The gap is $R_0 = 4.47$, so that the length of the pins in order to avoid impact is $l_p = 1.56$, both in dimensionless units. The outputs are, the rotor orbit, the impact force (if the rotor impacts the pins) and and the rotor angular velocity. After each simulation an additional algorithm is executed in order to guarantee that the transient response is not considered in the analysis. The minimum torque is the necessary torque for the rotor to surpass its critical angular velocity caused by the unbalance,

$$T_a \approx 1.3\left(\frac{\varepsilon}{R_g}\right)^{\frac{4}{3}}. \tag{7}$$

Then, in the rotational equation in (6), the torque term can again be rewritten in terms of minimum torque $\bar{\bar{T}} = \bar{T}/T_a$,

$$\theta'' = \bar{\bar{T}}T_a + \left(\frac{\varepsilon}{R_g}\right)^2 (Y\cos\theta - X\sin\theta) + \eta_i \left[\frac{2}{R_g^2}\left(\frac{\omega_p}{\omega}\right)^2 |\mathbf{d}\times\boldsymbol{\delta}|\left(1-\mu\frac{V^\star_{edge}}{|V^\star_{edge}|}\right)\right]. \tag{8}$$

From the numerical simulations, a bifurcation map of the maximum impact force at the pins can be generated, as shown in Figure 3, having the torque as control parameter. The bifurcation chart considers only the impact force peaks during each impact in permanent regime. Each simulation begins with the rotor at standstill, in other words, the initial conditions of the rotor are set to zero.

As indicated in the right edge of the graph in Figure 3, whenever the input torque is higher than 27.5 times the minimum torque, the rotor is capable of surpassing the critical speed without impacting any of the pins. For input torque values less than 1.5 times the minimum torque, the rotor stays in a orbit too small to collide with the pins and it does not surpass the critical angular velocity. Between these torque values it is possible to observe the rich non-linear behaviour the contact produces, including period-doubling bifurcations and chaotic behaviour. In the enlargement in Figure 3(a), it is seen that even a small range of torque may include a very rich dynamics of the impact force. In 3(b), one sees a small chaotic region which then develops into a bi-stable region. Moreover, there is some rough similarity between regions 3(a) and 3(b). The third detailed region, 3(c), comes after the second chaotic region, in which the disk trajectories converge to one major solution, but also a secondary orbit type was detected. Note that either the system stays on a main evolution in the center, or it describes a four contact force evolution.

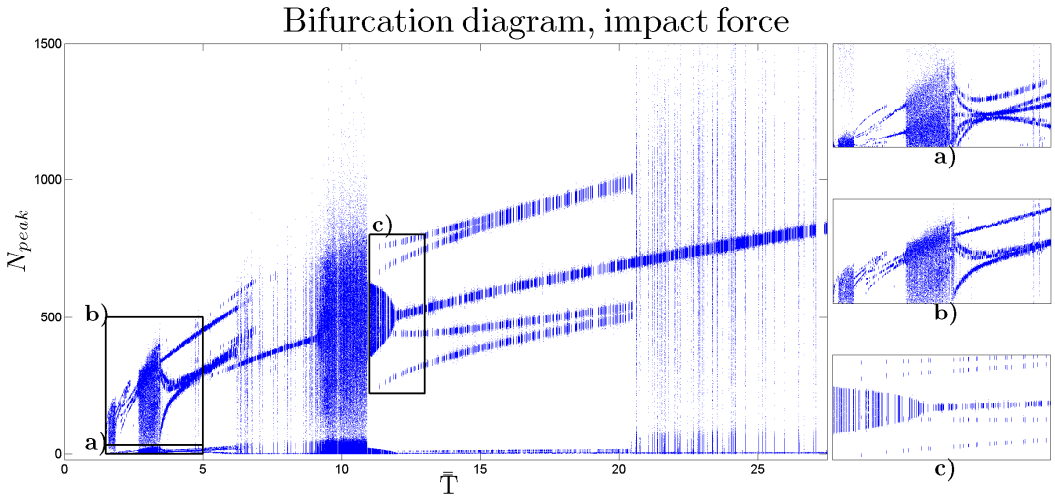

Figure 3: Bifurcation diagram of the maximum impacting force with enlargements of selected areas.

The bifurcation diagram is undoubtedly dependent of the clearance between the disk and the bearing and the length of the pins. With tighter pins, therefore with a smaller gap, the system was simulated and showed major chaotic orbits through the entire torque spectrum. If one plots the position of the impact points through the torque domain, we get the complex 3D diagram of Figure 4. Again we see the same features as in Figure 3 such as the chaotic region, bifurcation and separation regions and also multiple impacts on the left side of the graph. If one selects a constant torque and by plotting the position of the disk center of the simulation, it becomes clear that the disk moves through quasi-periodic trajectories in time inside the gap. It collides several times at the same pins and roughly at the same position. The interval between the minimum torque, $T/T_a = 1$ and $T/T_a = 27.5$ is the interesting part and different orbits appear including impacting continuously. Some of these orbits are shown in Figures 4(a) and 4(b). The coloured lines represent the enlightened trajectories for specific torques as demonstrations. In fact, there is a huge variety of orbits. Either the disk shows a star-shaped trajectory, or has the form of a horizontal/vertical biconvex geometry ('lemon'-shape) hitting only two pins, or complex forms at

lower values of torque. Some orbits do not show any quasi-periodicity, but a chaotic trajectory like the green curve in Figure 4(a) with $T/T_a = 10$ appears. Observe in Figure 4 a collection of the different orbits and one may notice that in a chaotic region $T/T_a = 9.5$ and $T/T_a = 10$, there also exist circular and stable orbits. This means that after a series of impacts, the disk reaches a stable-impactless-circular orbit when the applied torque is around $T/T_a = 9.86$. A slight difference in the torque leads to an orbit of circular or of a completely different shape.

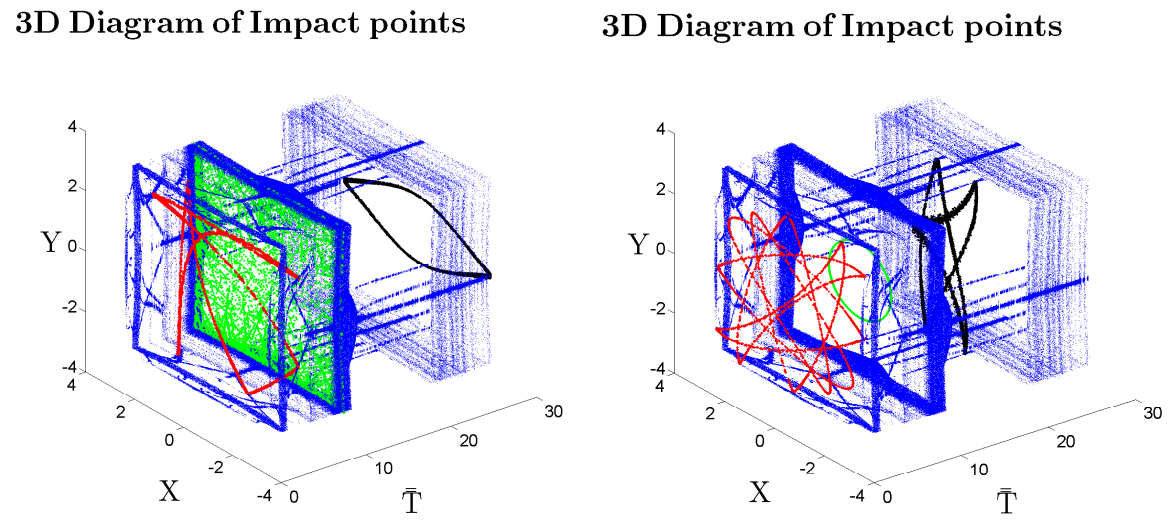

(a) (b)

Figure 4: At left: RED: $\bar{\bar{T}} = 5$. GREEN: $\bar{\bar{T}} = 10$. BLACK: $\bar{\bar{T}} = 27.5$.
At right: RED: $\bar{\bar{T}} = 1.9$. GREEN: $\bar{\bar{T}} = 9.86$. BLACK: $\bar{\bar{T}} = 19.5$.

Looking at the visual aspects of the orbits, a correlation between the bifurcation diagram and the quasi-periodic orbits can be done. If we analyse only from the chaotic region until the end of the bifurcation diagram, we have two stable trajectories, either a star-shaped orbit colliding in four points or the biconvex orbit. The main evolution in this section of the diagram represents the latter. The former one is given by the four branches that appear below and above. This correlation between the number of collision and the number of separate force values can be done with other torque values.

Part of this region was highlighted in Figure 3(c) to show the presence of two attractors. If the initial condition is changed, the trajectory geometry changes from one attractor to the other. This is seen in Figure 5, where, at left, the simulation starts from the standstill for all coordinates and the rotor develops a star orbit impacting four times on the pins. At right, the simulation started from a little lateral deviation $X = 1$. Now, the disk impacts only in two pins describing the biconvex trajectory.

We can determine which torque values were able to make the rotor follow a circular orbit by comparing the results of a new case without restrictions and impacts. Figure 6 shows the disk final angular velocity in both cases. The hypothetical one, in which the simulation is done without pins and bearing wall, is represented in the simulation by each of the small red circles, and the case which considers impacts in the simulation is represented by blue squares.

When both mark the same point, it means the final angular velocities are the same, and therefore, a safe circular orbit was achieved. In some numerical simulations throughout the domain, the rotor final angular velocity matches the simulations without pins. It means, in many cases, after a series of impacts, the rotor finally gets to a safer trajectory. In the end, the non-linearity effect of the impacts does not change much the capacity of the rotor to surpass its critical velocity, as the pins constrain the orbits and let the angular velocity increase over time. The simulations with pins (blue) achieved higher values of the angular velocity than the ones without them (red). We exhibit in Figure 6 the same features seen in the previous charts, which happen between $5 \leq T/T_a \leq 9$, where the coexistence of solutions is presented. Again, the same chaotic region is observed around $9 \leq T/T_a \leq 11$.

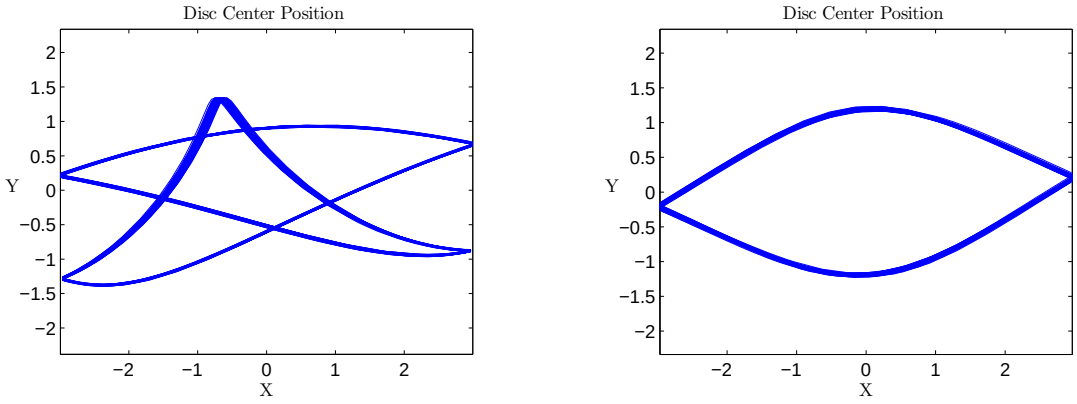

(a) (a)

Figure 5: Double stable orbits. Applied torque is $T/T_a = 14.45$. *Left*: All initial conditions are zero. *Right*: $X(t(0)) = 1$

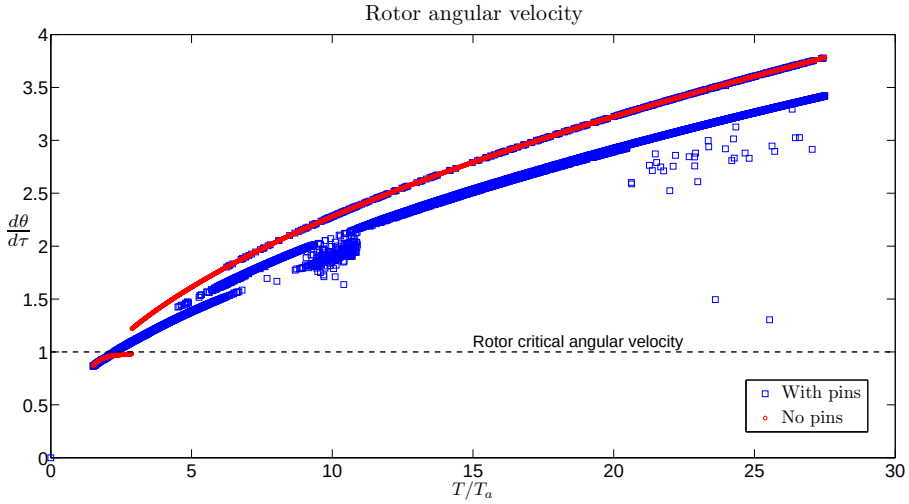

Figure 6: Final angular velocity with and without pins.

4 Experimental observations

As seen in Figure 1(b), an experimental test was built at the Dynamics and Vibration Laboratory at PUC-Rio. It is a vertical rotor with a slender shaft, driven from the top by AC motor with an inverter and carrying at the bottom a steel disk. Just above there it is a lighter disk made of aluminium that runs inside the retainer bearing containing the pins made of brass. The length of the pins is adjustable.

The rotor has three observable resonance frequencies. The first one, around $f_1 = 1.25$ Hz, is a rigid body resonance frequency and the rotor acts like a pendulum. The next two following frequencies, $f_2 = 23$ Hz and $f_3 = 75$ Hz, are natural beam frequencies carrying an inertia at the end. As expected, when the rotor is rotating in one of those frequencies, it develops an orbit with large amplitudes, till it reaches its limits due to the retainer bearing. At higher frequencies, not only it impacts, but also starts rubbing continuously and therefore the retainer bearing needs constantly to be replaced. In practical terms, hits and rubbing cause damage and wear to the structure and therefore the bearing must be constantly replaced.

To capture the trajectory of the rotor, four position eddy-current sensors were placed at the same level of the heavier disk, two for each coordinate in opposite sides. So the position is the mean between both measurements. Three data samples were collected with different acquisition frequencies. The first one was $T_s = 0.01s$ and the second and third ones were $T_s = 0.001s$. From rest, the AC motor was turned on and set to rotate at the rigid body frequency. Soon orbits became higher and higher and started to hit the pins. The trajectory described a 'star'-like shape colliding in all pins, Figure 7.

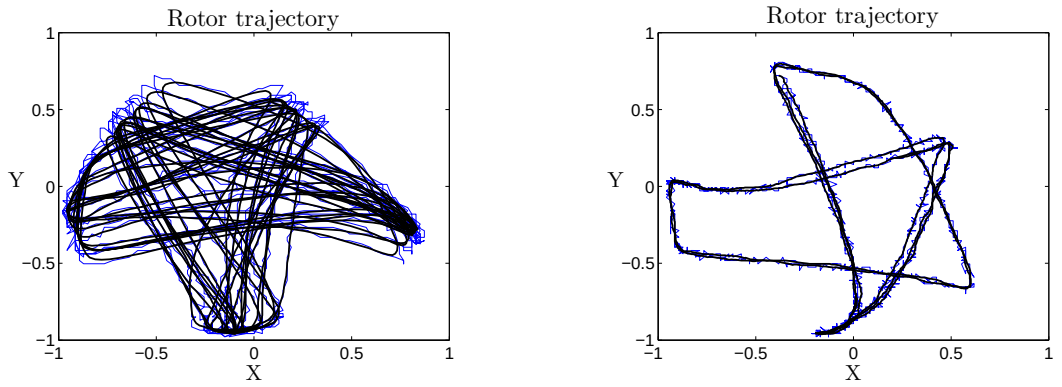

(a) (b)

Figure 7: (a) Longer sample of the trajectory $T_s = 0.01s$. (b) Shorter sample of the trajectory, but more precise $T_s = 0.001s$. The dark line is a moving average of the rotor.

When the rotor was stopped and set to rotate again, the rotor's orbit did not acquire the previous shape, but rather a more rectangular path, colliding at each pin sub-sequentially, see Figure 8.

This last orbit is a stronger attractor since it is easier to obtain, clearly dependent on the initial position. Also, no great perturbation on the angular velocity was observed. At other critical angular velocities of the rotor, when the disk impacts on the pins it starts colliding chaotically.

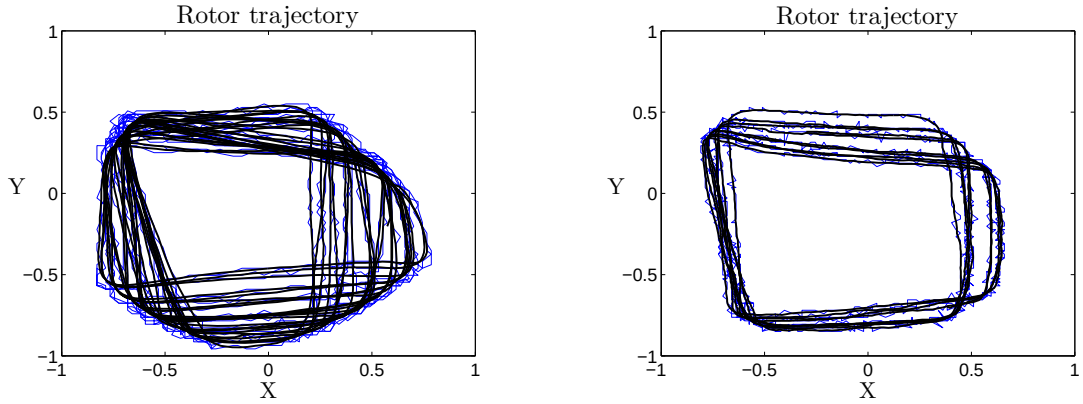

(a) (b)

Figure 8: (a) Longer sample of the trajectory $T_s = 0.01s$. (b) Shorter sample of the trajectory, but more precise $T_s = 0.001s$. The dark line is a moving average of the rotor.

A second and definite observation of the effectiveness of the pins is shown in Figure 9. Here, the rotor starts from the standstill and is accelerated by a low torque motor until it reaches 7.5 Hz, far beyond the first natural frequency. The only difference between both experiments that were done is that in the ones at right of the figure, the pins were removed from the bearing and it becomes an ordinary circular bearing. At left, we see that the rotor starts impacting a little bit before than in the experimental result at right. As the angular velocity increases till the first natural frequency, the orbit size increases considerably. Afterwards the rotor is able to loose itself from this impacting orbit and accelerates. The same does not happen when the pins are not present. The rotor rubs on the bearing wall, shakes the structure harshly and the angular velocity stays below the desired value and even goes to zero.

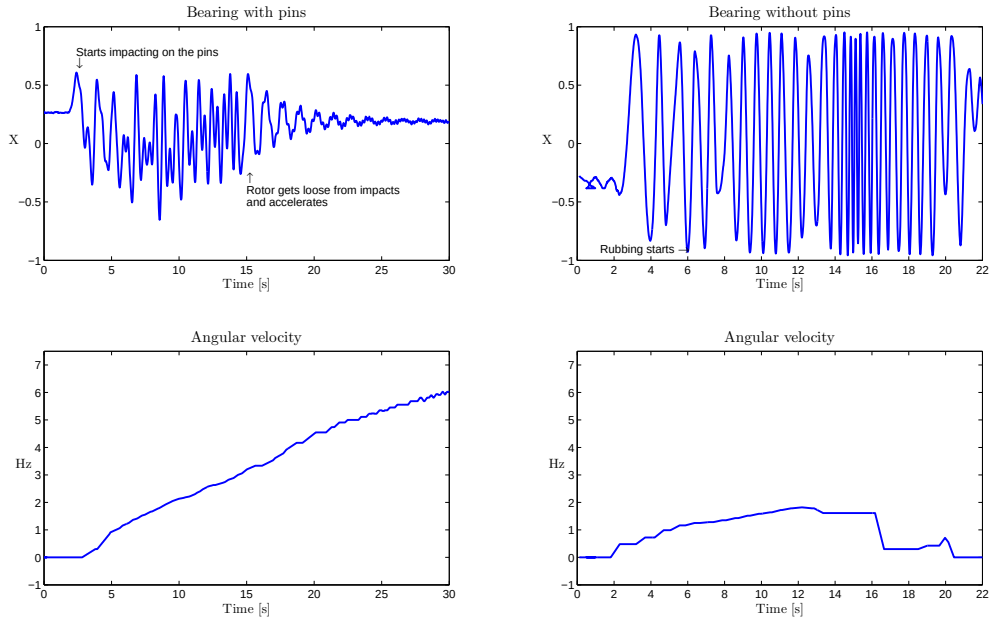

Figure 9: Lateral and angular velocity of the rotor with and without the pins.

5 Conclusion

The use of pins in safety bearings is a new way to limit rotor lateral amplitudes and therefore to reduce damage to rotors, specially during rotor start ups. Published works have already shown the validity of the use of pins in [9, 14]. Numerical simulations showed that a DeLaval rotor, during start up, constrained by such a safety bearing with pins exhibit a series of different and interesting orbits, whose behaviour depends on the gap and the torque applied. As the applied torque varies, the system intercalates quasi-periodic orbits in different shapes and chaotic behaviour. When displaying the bifurcation diagram using the rotor impact force on the safety bearing, a vast and rich non-linear behaviour occurs, such as period-doubling bifurcations and constant changes of basins of attraction. Chaotic regions and two-stable orbits could be seen together with a small region where the pin did help the rotor to develop into a more stable circular orbit. Also, the angular velocity in the steady state is plotted against the torque applied, showing that the non-linear effect of the impacts does not change the capacity of the rotor to surpass its critical velocity, as the pins constrain the orbits and let the angular velocity to advance over time.

Moreover, the experimental analysis showed that some of the simulated orbits can be obtained at the test rig. The star-shaped trajectory and other regular orbits do exist, which gives a good validation of the impact model defined in the present and previous works, equation (3). Since the angular velocity does not alter significantly when the pins are inside the structure, the use of such a device is once again proven to help to the rotor to surpass known critical speeds and to avoid strong impacts and rubbing. Although the minimum torque became quite big, the gap is, on the other hand, small.

For future analysis, the modelling of the system will be changed and, instead of a back-up bearing with pins, an impact on a ball bearing model will be included. The ball bearings are the current used device to withstand the impact of a rotor in industrial applications. So it is intended to give a final approach to the problem and therefore a good comparison between the bearings.

6 Acknowledgements

This work was supported by the Brazilian Agency CNPq.

References

[1] Muszynska, A., (2005), Rotordynamics. CRC Press, USA.

[2] Fumagalli, M., Schweitzer, G. (1996). Motion of a Rotor in Retainer Bearings. *Fifth International Symposium on Magnetic Bearings*, Kanazawa, Japan.

[3] Schweitzer G., Stabilization of self-excited rotor vibration by an active damper., *Dynamics of Rotors - IUTAM Sympoisum*, 1974, Lyngby, Denmark.

[4] Ulbrich H., Schweitzer G., Bauser E., A rotor supported without contact theory and application. *Proceedings of the Fifth World Congress on Theory of Machines and Mechanisms*, 1979.

[5] G. Wegener, R. Markert and K. Pothmann (1998). Steady-State-Analysis of a Multi-Disk or Continuous Rotor with one Retainer Bearing. *IFToMM Fifth International Conference on Rotor Dynamics*, Darmstadt, Germany.

[6] Schmied, J., Pradetto J.C., Behaviour of a one ton rotor being dropped into auxiliary bearings. *Proceedings of the Third International Symposium on Magnetic Bearings*, 145-156.

[7] Ginzinger, L., Heckmann, B., Ulbrich, H., Feedback control to prevent damage by rotor rubbing after an imipact load. *Proceedings of ASME Turbo Expo*, 2007, Vol. 129, 522-529.

[8] Ecker, H. (1998). Nonlinear Stability of a Single Mass Rotor Contacting a Rigid Auxiliary Bearing. *IFToMM Fifth International Conference on Rotor Dynamics*, Darmstadt, Germany.

[9] Fonseca, C.A., Weber, H.I., Fleischer, P.F., Santos, I.F. (2013). Analyzing the use of pins in safety bearings. *10th International Conference on Vibrations in Rotating Machines*, Berlin, Germany.

[10] Fonseca, C.A. (2013) Analyzing the use of active pins in safety bearings. *Master Dissertation*, Mech.Eng. Dept., PUC-Rio, Rio de Janeiro, Brazil.

[11] Fonseca, C.A., Romulo R. Aguiar, Hans I. Weber (2014) Numerical study of a rotor/ stator contact behaviour using a new containment bearing design, *8th European Nonlinear Dynamics Conference* (ENOC 2014), Vienna, Austria.

[12] Gasch, R. , Nordmann, R. , Pfützner, H., (2002), *Rotordynamik* Berlin, 2nd ed., Springer Verlag

[13] Isaksson, J.L. (1994). *On the dynamics of a rotor interacting wih non-rotating parts*. Linköping: Linköping of Studies in Science and Technologies.

[14] S. Lahriri , H. Weber, I Santos and Henning Hartmann, Rotor-stator contact dynamics using a non-ideal drive-Theoretical and experimental aspects. Journal of Sound and Vibration 331 (2012) 4518-4536.

[15] S. Lahriri, I. Santos, H Weber, et al., On the nonlinear dynamics of two types of backup bearings-theoretical and experimental aspects. *Journal of Engineering for Gas Turbines and Power* 134 (2012): 112503.1 - 112503.13.

[16] Simon, U. (2000). *Rotor-Stator-Kontakt in polygonförmigen Fanglagern*. Doctorate Thesis, TU Braunschweig.

[17] Markert, R., Pfützer, H., Gasch, R. (1980) Mindestantriebsmoment zur Resonanzdurchfahrt von unwuchtigen elastischen Rotoren. *Forschung im Ingenieurwesen* 46(2):33-46.

[18] H. Ma, C. Shi, Q. Han, et al., Fixed-point rubbing fault characteristic analysis of a rotor system based on contact theory. Mechanical System and Signal Processing 38 (2013) 137-153.

[19] A. Chavez, H. Ulbrich, L. Ginzinger, Reduction of contact forces in a rotor-stator-system in case of rubbing through active auxiliary bearing, *Shock and Vibration*, 2006, 13: 505-518.

[20] Steven H. Strogatz, Nonlinear Dynamics and Chaos: with Applications to Physiscs, Biology, Chemistry and Engineering, Westview Press, 1994.